AD-A179 547    AL AND MG ALLOYS FOR AEROSPACE APPLICATIONS USING RAPID    1/1
               SOLIDIFICATION AN. (U) ILLINOIS UNIV AT URBANA DEPT OF
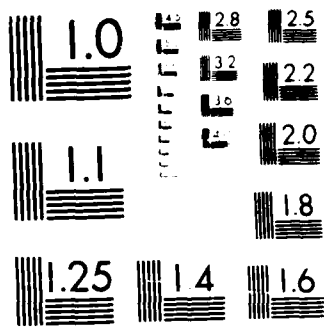               METALLURGY AND MINING ENGINEE.    FRASER MAY 87
UNCLASSIFIED   AFOSR-TR-87-0421 AFOSR-85-0191                F/G 11/6    NL

MICROCOPY RESOLUTION TEST CHART

NATIONAL BUREAU OF STANDARDS

# REPORT DOCUMENTATION PAGE

| 1a. REPORT SECURITY CLASSIFICATION UNCLASSIFIED | 1b. RESTRICTIVE MARKINGS |
|---|---|
| 2a. SECURITY CLASSIFICATION AUTHORITY | 3. DISTRIBUTION/AVAILABILITY OF REPORT |
| 2b. DECLASSIFICATION/DOWNGRADING SCHEDULE | Unlimited distribution |

| 4. PERFORMING ORGANIZATION REPORT NUMBER(S) | 5. MONITORING ORGANIZATION REPORT NUMBER(S) AFOSR-TR- 87-0421 |
|---|---|

| 6a. NAME OF PERFORMING ORGANIZATION Univ. of Illinois | 6b. OFFICE SYMBOL (If applicable) | 7a. NAME OF MONITORING ORGANIZATION AFOSR |
|---|---|---|
| 6c. ADDRESS (City, State and ZIP Code) Dept of Metallurgy & Mining Engineering 1304 West Green Street Urbana Illinois 61801 | | 7b. ADDRESS (City, State and ZIP Code) Bolling AFB WASH DC Blg 410 |
| 8a. NAME OF FUNDING/SPONSORING ORGANIZATION AFOSR | 8b. OFFICE SYMBOL (If applicable) NE | 9. PROCUREMENT INSTRUMENT IDENTIFICATION NUMBER AFOSR-85-0191 |

APR 24 1987

DTIC SELECTED S E

| 8c. ADDRESS (City, State and ZIP Code) same as 7b | 10. SOURCE OF FUNDING NOS. |
|---|---|

| PROGRAM ELEMENT NO. | PROJECT NO. | TASK NO. | WORK UNIT NO. |
|---|---|---|---|
| 61102F | 2306 | A1 | |

11. TITLE (Include Security Classification)
Al & Mg Alloys for Aerospace Applications Using Rapid Solidification & Powder Metallurgy Processing

12. PERSONAL AUTHOR(S)
Fraser

| 13a. TYPE OF REPORT Annual | 13b. TIME COVERED FROM 5-15-86 TO 5-15-87 | 14. DATE OF REPORT (Yr., Mo., Day) | 15. PAGE COUNT |
|---|---|---|---|

16. SUPPLEMENTARY NOTATION
→ molybdenum alloys, aluminum alloys, ← silicon Iron alloys

| COSATI CODES | | | 18. SUBJECT TERMS (Continue on reverse if necessary and identify by block number) |
|---|---|---|---|
| FIELD | GROUP | SUB. GR | |

Progress:

NARR. -- PROG. - FROM U) silicon
May 15 86 to May 15 87

19. ABSTRACT (Continue on reverse if necessary and ...

The first section of the progress report is concerned with the development of rapidly solidified Al-8Fe-2Mo-Si alloys for elevated temperature applications. Rapidly solidified Al-8Fe-2Mo alloys containing Si in the range of 0 to 1wt pct were produced by melt spinning. In the second annual report, preliminary results of the effect of Si on the formation of the Zone A microstructure and on subsequent changes of this structure during heat-treatment were described. It was shown that addition of Si has a dramatic effect on the transformation behavior and microstructure of heat-treated ribbons. In contrast to the thermally unstable, multiphase precipitate distribution in the ternary Al-8Fe-2Mo alloy, quarternary Si-containing alloys showed a uniform dispersion of fine cuboidal/polygonal precipitates, which displayed a remarkable resistance to coarsening. A typical TEM micrograph portraying this effect is shown in Fig. 1 for a Al-8Fe-2Mo-0.5Si alloy heat treated at 450°C for 50 hrs. To identify the nature of the precipitates, x-ray and electron diffraction were used, and these results are reported here.

| 20. DISTRIBUTION/AVAILABILITY OF ABSTRACT UNCLASSIFIED/UNLIMITED ☒ SAME AS RPT ☐ DTIC USERS ☐ | 21. ABSTRACT SECURITY CLASSIFICATION UUUUU |
|---|---|
| 22a. NAME OF RESPONSIBLE INDIVIDUAL Dr. Alan Rosenstein | 22b. TELEPHONE NUMBER (Include Area Code) 767-4931 | 22c. OFFICE SYMBOL NE |

DD FORM 1473, 83 APR    EDITION OF 1 JAN 73 IS OBSOLETE.

AD-A179 547

# Al AND Mg ALLOYS FOR AEROSPACE APPLICATIONS USING RAPID SOLIDIFICATION AND POWDER METALLURGY PROCESSING

The first section of the progress report is concerned with the development of rapidly solidified Al-8Fe-2Mo-Si alloys for elevated temperature applications. Rapidly solidified Al-8Fe-2Mo alloys containing Si in the range of 0 to 1 wt pct were produced by melt spinning. In the second annual report, preliminary results of the effect of Si on the formation of the Zone A microstructure and on subsequent changes of this structure during heat-treatment were described. It was shown that addition of Si has a dramatic effect on the transformation behavior and microstructure of heat-treated ribbons. In contrast to the thermally unstable, multiphase precipitate distribution in the ternary Al-8Fe-2Mo alloy, quarternary Si-containing alloys showed a uniform dispersion of fine cuboidal/ polygonal precipitates, which displayed a remarkable resistance to coarsening. A typical TEM micrograph portraying this effect is shown in Fig. 1 for a Al-8Fe-2Mo-0.5Si alloy heat-treated at 450°C for 50 hrs. To identify the nature of the precipitates, x-ray and electron diffraction were used, and these results are reported here.

X-ray diffraction experiments were carried out on the Rigaku D-max diffractometer using Cu $K\alpha$ radiation. Heat-treated ribbons (450°C, 50 hrs) of the 0.5 and 1 wt pct Si alloys were mounted on a glass slide, placed in the diffractometer chamber, and the patterns recorded. A typical variation of the Intensity (cps) as a function of $2\theta$ is shown in Fig. 2 for the 1 wt pct Si alloy. All the precipitate reflections could be consistently indexed on the basis of a bcc lattice with $a_0 = 1.263\pm0.004$ nm, which closely matches the value of 1.252 nm for the bcc $\alpha$-AlFeSi compound. This compound is stablized by a quarternary element—in this case—Mo.

Electron diffraction experiments were carried out to confirm the x-ray results. Examples of diffraction patterns recorded from individual precipitates are shown in Fig. 3. These and all other patterns could be consistently indexed on the basis of a bcc lattice with a lattice parameter nearly identical to that determined by x-ray diffraction.

To determine the point group and space group of the precipitates, convergent beam electron diffraction (CBED) was used. CBED patterns of the [001], [023], and [111] zone axes are shown in Figs. 4—6. The bcc Bravais lattice for the precipitates is once again confirmed from the [001] pattern. For a bcc lattice, the ratio of the spacings of the FOLZ and ZOLZ is equal to $\sqrt{2}$. Measurements of these spacings from the patterns in Fig. 4 gave $d_{FOLZ}/d_{ZOLZ} = 12.6/9.03 = 1.4 \approx \sqrt{2}$, thus confirming the bcc lattice. Symmetry information deduced from the CBED patterns in Figs. 4—6 was compared to tables provided by Buxton et al. The results are summarized in Table 1. For the [001] orientation, the projection diffraction and whole pattern symmetries are 2mm, which places the diffraction group as 2mm or $2mm1_R$. For the [023] zone axes, the projection diffraction, whole pattern and bright field (BF) symmetries are 2mm, m, and m, respectively,

which gives $2_R mm_R$ as the diffraction group. For the [111] zone axes, the projection diffraction and whole pattern symmetries are 6 and 3, respectively, which gives the diffraction group as $6_R$. The possible point groups corresponding to the above diffraction groups is summarized in Table 2, from which it is established that the point group of the precipitates is m3.

The possible space groups for this point group are Pm3, Pn3, Pa3, Fm3, Fd3, Im3, and Ia3. Since the lattice is bcc, the choice of space groups is reduced to the last two, namely, Im3 or Ia3. For the latter space group, reflections of type 0kl for which k and l are not multiples of 2, that is, of type 011, 033 ..., are not allowed, which is not the case here. Thus, the space group of the precipitates is unambiguously established as Im3.

Current work is directed at determinations of the chemical composition , volume fraction, and orientation relationships, if any, of the precipitates. In additon, as-rapidly solidified ribbons have been reduced to particulate to produce extrusions for determinations of the tensile strength and fracture toughness at both room and elevated temperatures; the fatigue properties will also be evaluated. Studies of dislocation-particle interactions will also be undertaken to determine the strengthening mechanism.

TABLE 1

| Zone Axes | Observed Symmetry | | | Deduced Diffraction Group |
|---|---|---|---|---|
| | Projection | Whole Pattern | BF | |
| [001] | 2mm | 2mm | - | 2mm or 2mm1$_R$ |
| [023] | 2mm | m | m | 2$_R$mm$_R$ |
| [111] | 6 | 3 | - | 6$_R$ |

TABLE 2

| Deduced Diffraction Groups | Possible Point Groups | | | | | | | |
|---|---|---|---|---|---|---|---|---|
| 2mm | mm2 | | 6m2 | | | | | |
| 2mm1$_R$ | | mmm | 4mmm | 6/mmm | | | m3 | m3m |
| 2$_R$mm$_R$ | 2/m | mmm | 4/m 4mmm | 6/mmm | 3m | 6m | m3 | m3m |
| 6$_R$ | | 3 | | | | | m3 | |

The second section of this progress report covers work performed on Mg-Si alloys. A preliminary investigation of these alloys revealed several interesting features which may be exploited using rapid solidification techniques. Mg alloys containing 0.5, 1, 2, 3, 4, 5, 6, and 8 wt pct Si have been produced; a major focus of the study has been on alloys containing 1, 3, 5 and 8 wt pct Si. These specific compositions were chosen to investigate the effect of rapid solidification on both hypoeutectic and hypereutectic alloys and to generate a metastable Mg-Si phase diagram. This study draws heavily on that performed on Al-Ni and Al-Co alloys during previously supported AFOSR work. Both laser surface melting (LSM) using a continuous $CO_2$ laser and melt spinning into ribbon (MSR) in an inert gas atmosphere have been used to produce rapidly solidified material. LSM produced excellent results in alloys containing over 2 wt pct Si; for Si contents of 2 wt pct and lower, the melt pools were irregular and blow holes were common (perhaps due to the high vapor pressure of pure Mg). Therefore, in order to achieve consistent results, the bulk of the study was carried out on the more uniform melt spun ribbon. The melt spun material was studied in both the as-solidified condition and after various heat treatments.

Melt spun ribbons were quite uniform and were produced in one continuous strand. Alloys containing less than 2 wt pct Si had rougher edges and also tended to stick to the surface of the mild steel wheel, whereas those containing higher Si were uniformly single strand with smooth edges and sides. Several interesting observations were made during the production of the ribbons. As the Si content of the alloy increased, the ribbons became an increasingly darker shade of lavender. Since the color of $Mg_2Si$ is a dark purple, this effect was attributed to an increased $Mg_2Si$ content in the ribbons. Another observation was that the casting behavior of the alloys improved with increasing amounts of Si; alloys containing upto 2 wt pct Si had an average ribbon thickness of 73 $\mu m$, whereas those containing higher Si had an average thickness of 48 $\mu m$. The improvement in castability of the melt can be attributed to the lowering of the viscosity by the addition of Si. This is taken as an explanation for the improvement in ribbon quality and reduction in thickness with an increase in Si content. This result has also been observed in Al-Si alloys. The as-melt spun ribbon was quite ductile for Si contents upto 2 wt pct, whereas those containing higher amounts of Si, with the exclusion of the 5 wt pct alloy, were prone to cracking on bending. The 5 wt pct alloy was the most ductile of all the ribbons, and this enhanced ductility was later determined to result from a novel microstructure produced using rapid solidification.

Microhardness measurements were made on ribbons both as-melt spun and after heat-treatment upto 72 hrs. The ribbons were placed edgewise in clay and mounted in epoxy. After careful polishing, the microhardness was measured from the center of each ribbon. Although the values obtained using this method may not be directly comparable to values of the bulk material, they can be used to compare the hardness of different alloy ribbons providing they are all prepared in the same manner. Fig. 7 shows the variation in the microhardness of the Mg alloys as a function of composition. It can be seen that the microhardness increases upto 5 wt pct Si and then decreases at higher Si contents. The drop in hardness above 5 wt pct Si was unexpected and therefore,

microstructural examinations of the as-spun ribbons was undertaken to determine the cause for this effect. Optical micrographs of the Mg-5 wt pct Si alloy in the as-cast and as-melt spun conditions are shown in Figs. 8a and 8b, respectively. The latter microstructure may be considered as a metastable microeutectic between Mg and $Mg_2Si$. The degree of refinement of the individual primary intermetallic $Mg_2Si$ in the melt spun ribbon is approximately $10^5$ compared to those in the as-cast material; the eutectic microstructure is correspondingly refined by a factor of $10^3$. More importantly, the microstructure of the melt spun ribbon is uniform, with no evidence of primary intermetallic particles at the grain boundaries. Moreover, no evidence is seen for a precipitate free zone at the grain boundaries.

The microstructure of the other Mg-Si melt spun alloys was also examined; these results are summarized below. In the ribbons containing 1 and 3 wt pct Si, the microstructure was cellular (dendritic) with eutectic $Mg_2Si$ present at the grain boundaries. A supersaturation of Si existed in the Mg matrix, but an accurate value has not been obtained yet. The metastable supersaturation has been estimated at about 0.25 wt pct Si, and this value appears to decrease with increasing Si contents in the alloy. The microstructure of the 4 wt pct Si alloy consisted of a few Mg cells surrounded by a irregular network of rod-like Mg- $Mg_2Si$ eutectic. While the 5 wt pct Si alloy possessed a uniform coupled eutectic microstructure, the alloy containing 6 wt pct Si had a irregular network of rod-like Mg-$Mg_2Si$ eutectic surrounding fine primary $Mg_2Si$ crystals. Finally, the microstructure of the melt spun 8 wt pct Si alloy consisted of primary dendritic $Mg_2Si$ crystals with fine eutectic, with the scale of the dendrite arms ten times larger than that of the eutectic.

The microstructures observed may be explained using current theories involving undercooling and a asymmetrical coupled eutectic zone. The behavior is similar to that of Al-Co and Al-Ni alloys described in previous annual reports. As the degree of undercooling increases, the region of eutectic growth shifts toward more enriched alloy compositions. In dilute alloys, the primary phase nucleates first and rejects solute into the interdendritic regions, where the eutectic forms. This is observed in alloys with a composition upto 4 wt pct Si. The uniform eutectic forms in the 5 wt pct Si alloy due to cooperative growth between the phases at a specific undercooling. Finally, at compositions between 5 and 6 wt pct Si, fine primary $Mg_2Si$ crystals form first, followed by an irregular eutectic.

The thermal stability of these microstructures is currently under investigation. Melt spun alloy ribbons having the coupled eutectic microstructure will be produced, reduced to particulate and then extruded to determine the mechanical properties.
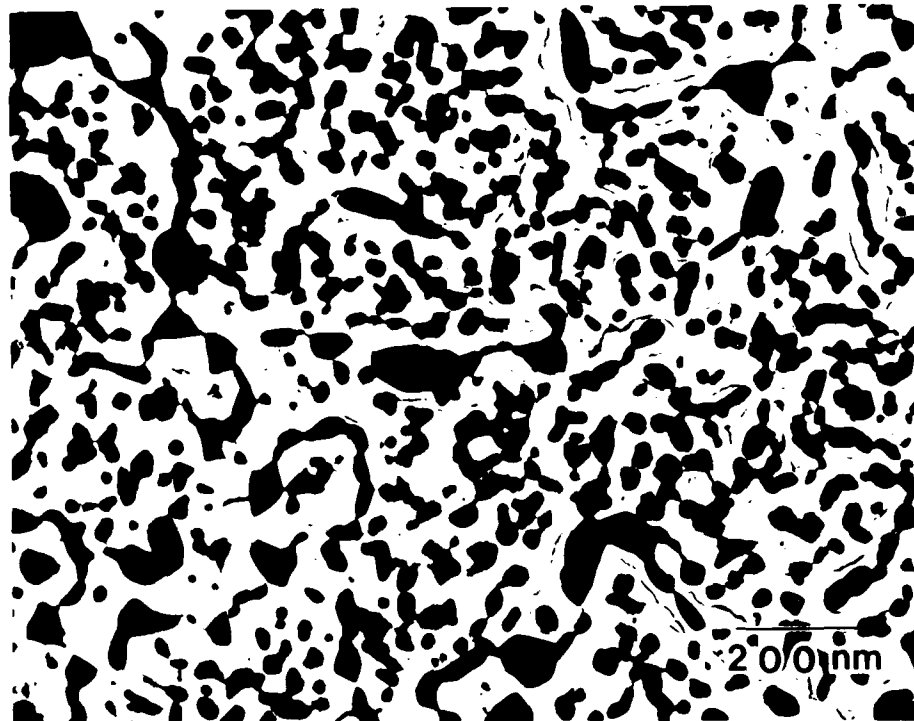
Fig. 1. TEM micrograph of Al-8Fe-2Mo-0.5Si alloy ribbon heat-treated at 450°C for 50 hrs.
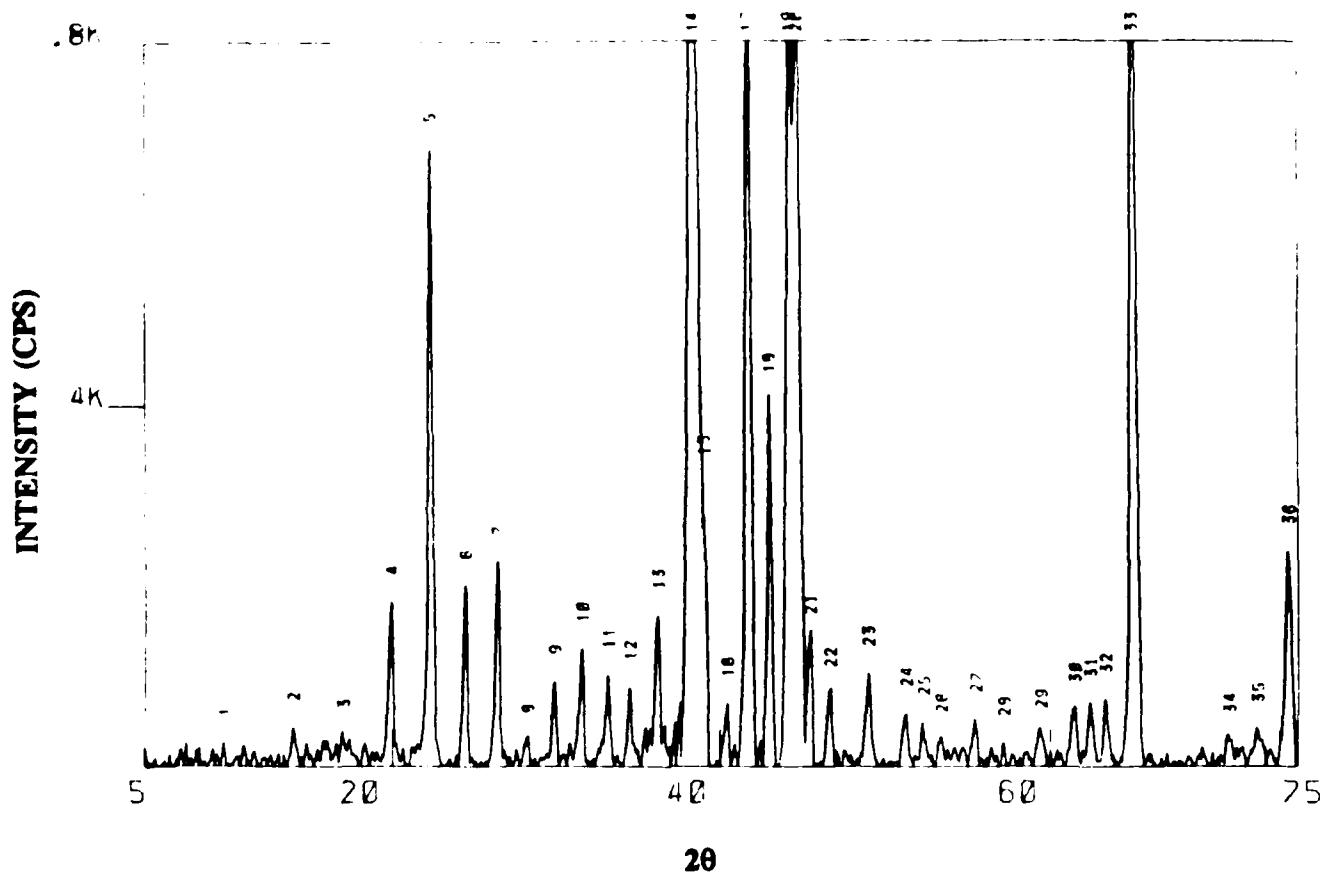
Fig. 2. Variation of x-ray intensity (CPS) as a function of 2θ of the Al-8Fe-2Mo-1Si alloy heat-treated at 450°C for 50 hrs.
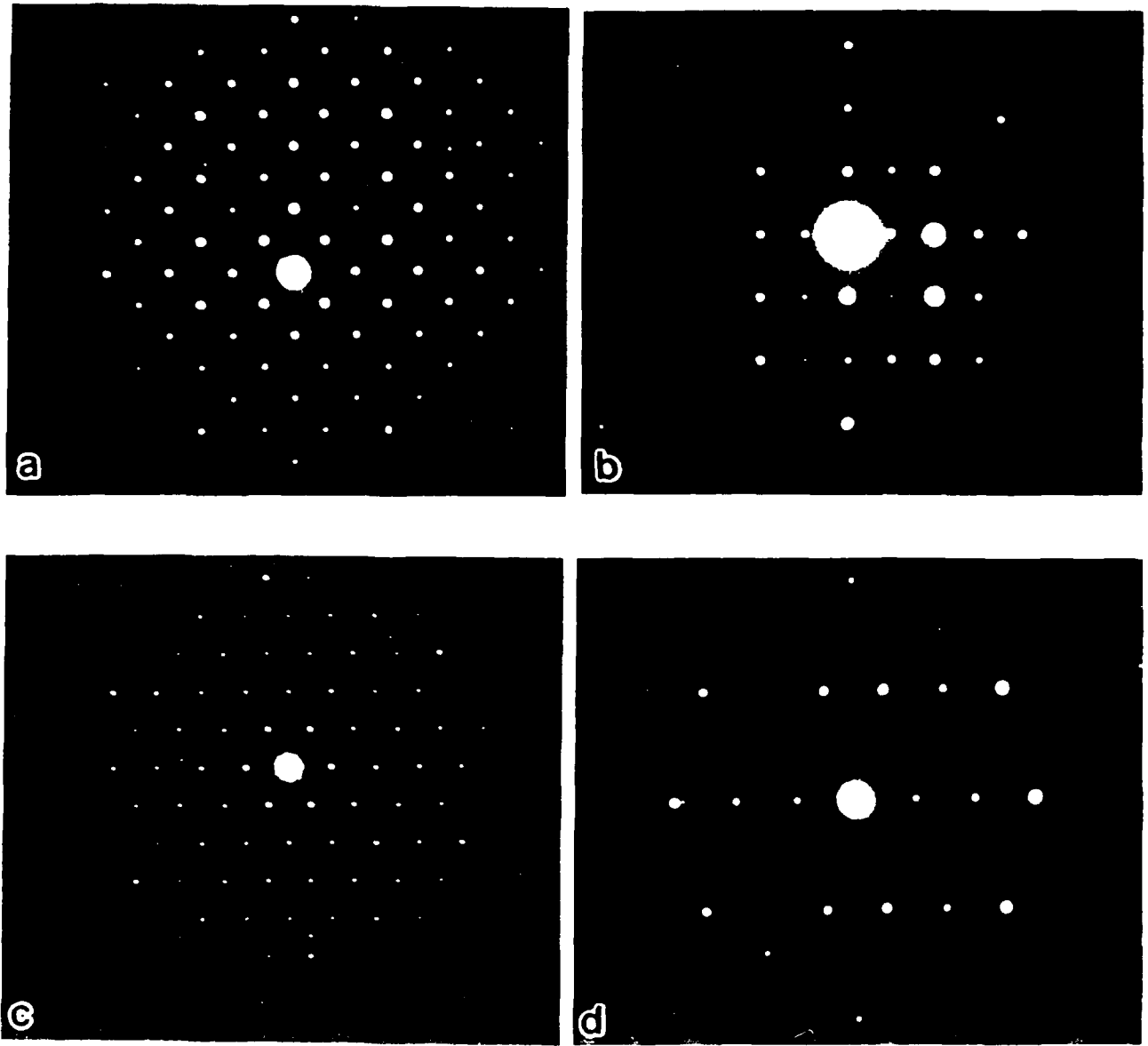
Fig. 3. Examples of diffraction patterns taken from individual precipitates. a) [001]; b) [011]; c) [111] and d) [023].
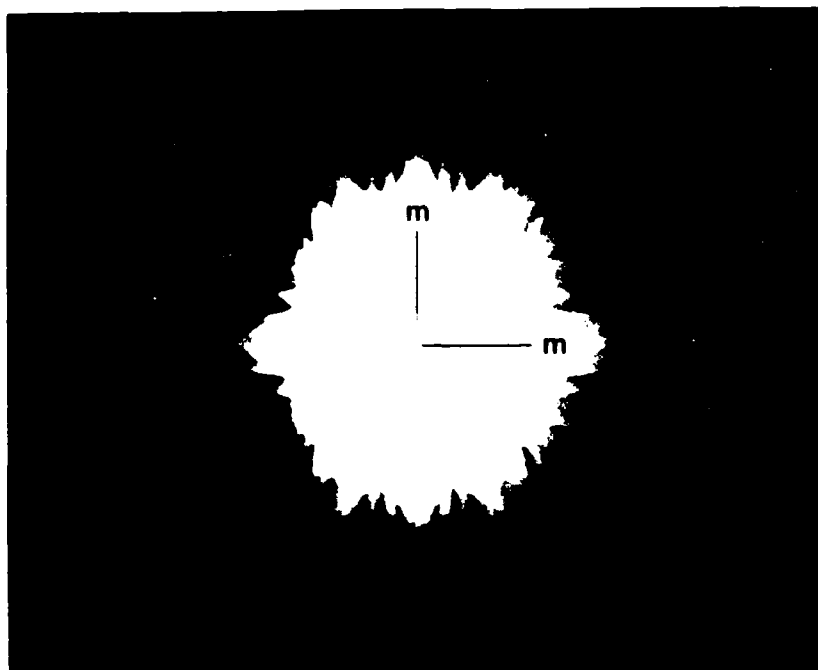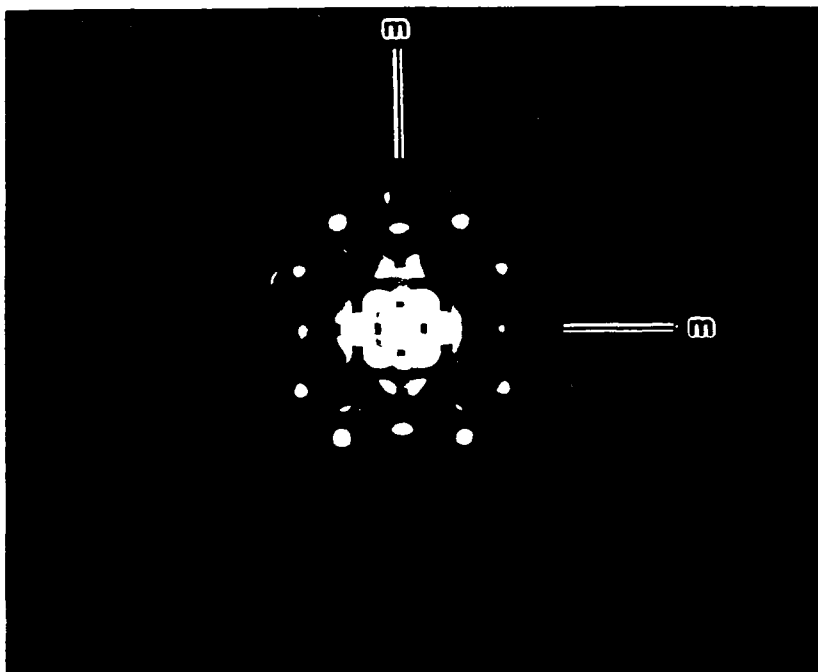
Fig. 4. [001] CBED pattern showing 2mm projection and whole pattern symmetries.
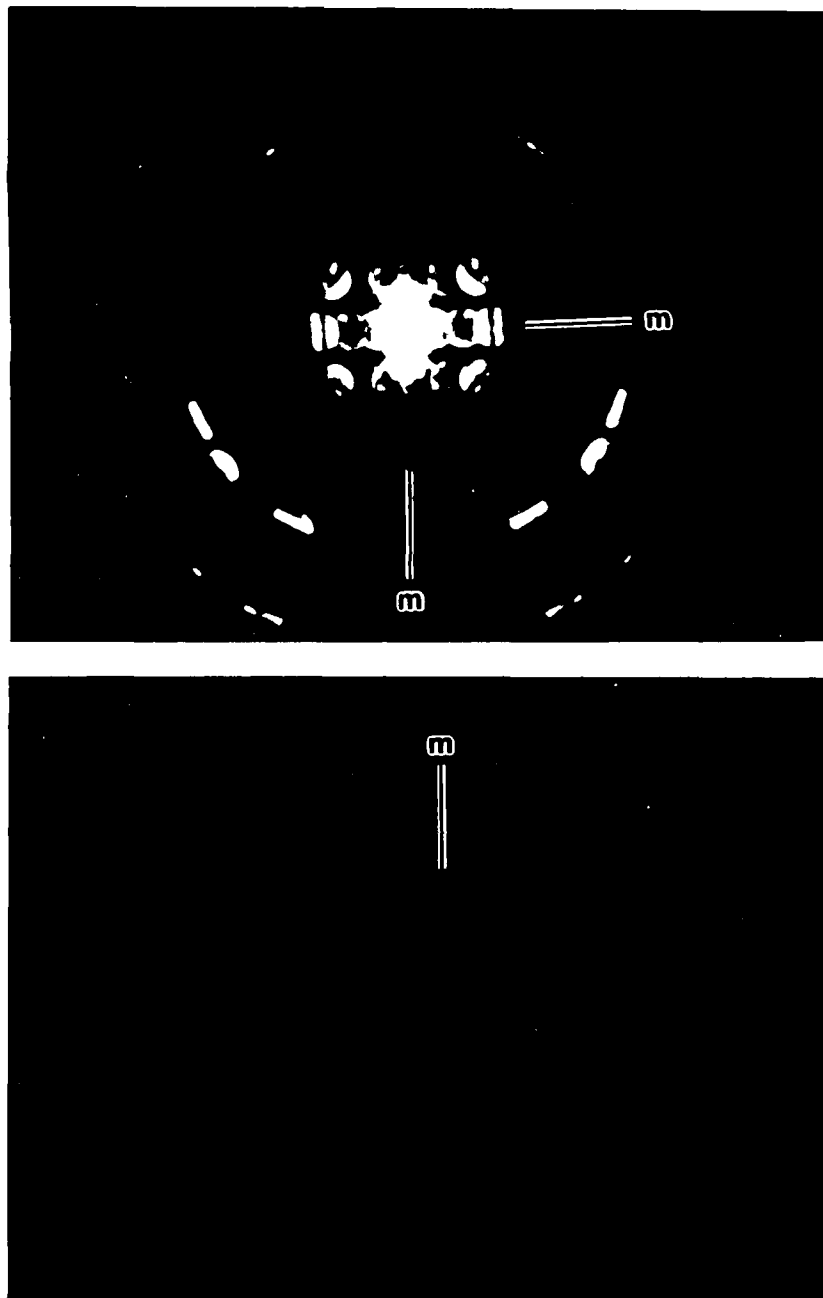
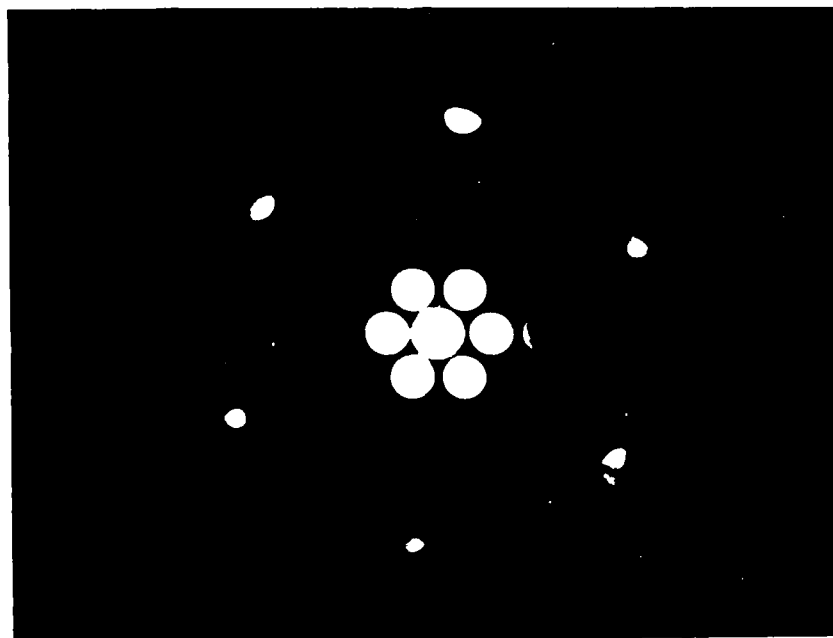Fig. 5. [023] CBED pattern showing 2mm projection symmetry and m whole pattern and bright field symmetries.
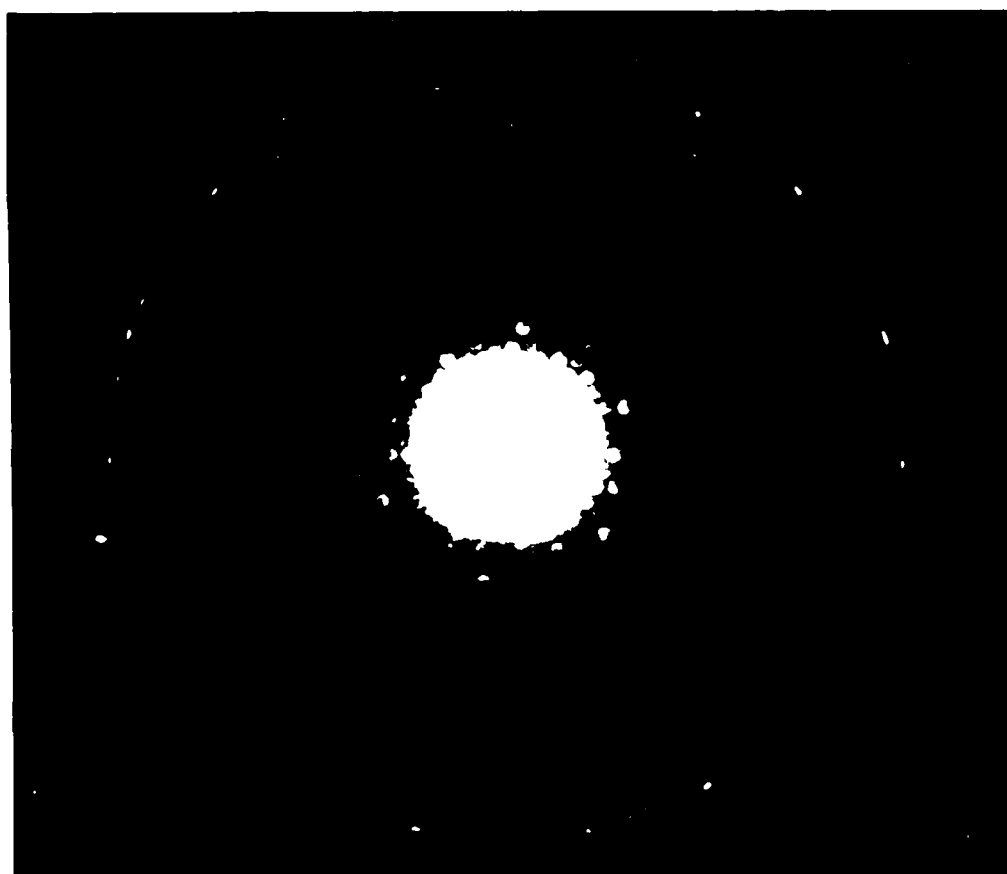
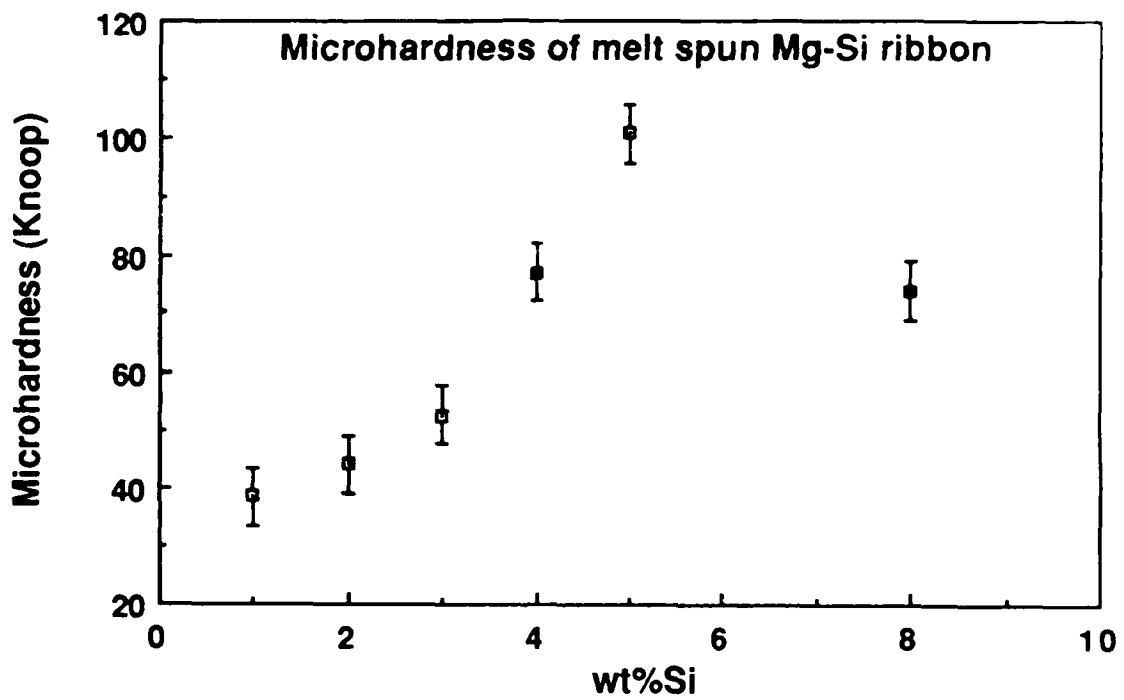Fig. 6. [111] CBED pattern showing 6 and 3 projection and whole pattern symmetries, respectively.
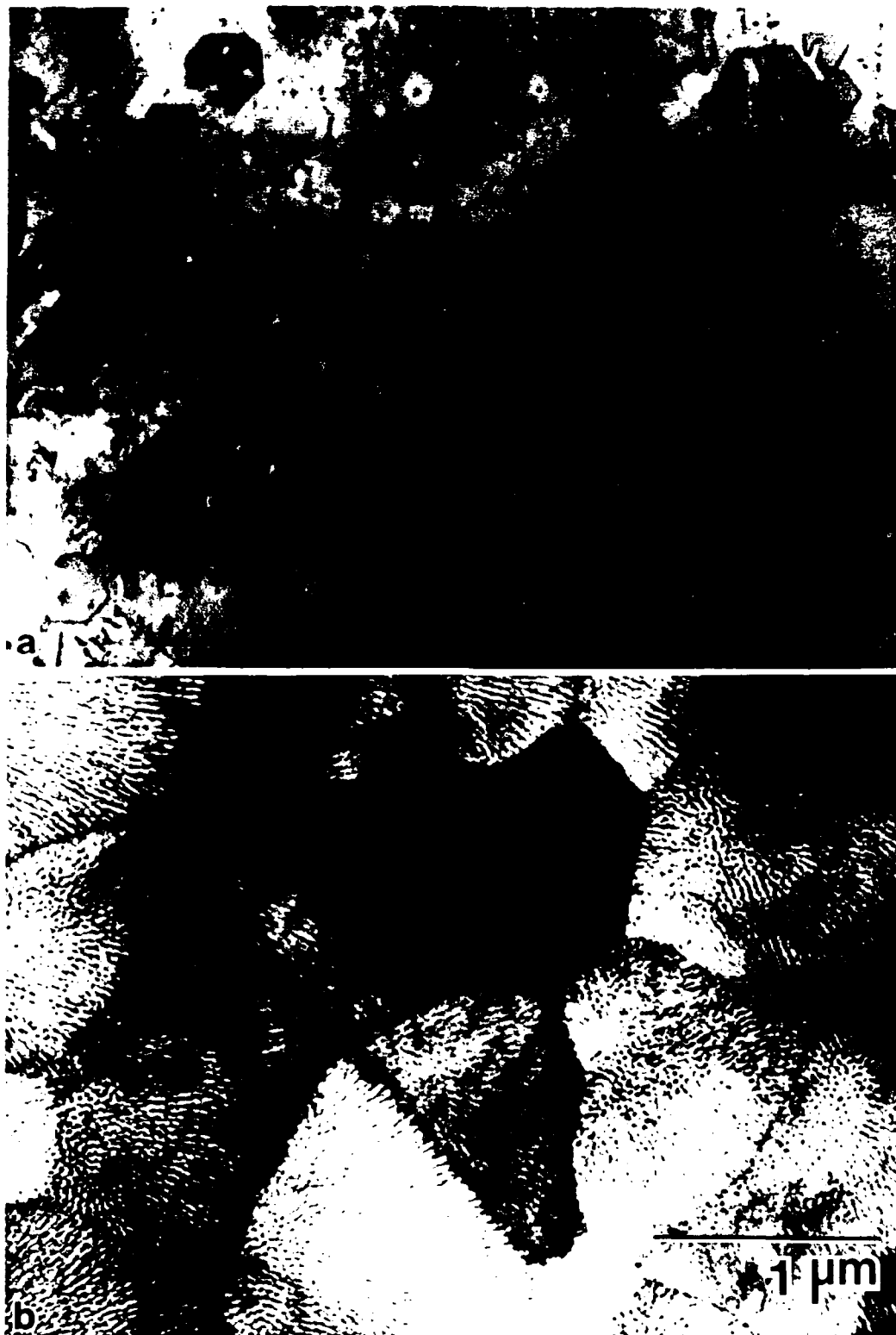
Fig. 7. Microhardness of melt spun Mg-Si alloys.

Fig. 8. Microstructures of the Mg-5 wt pct Si alloy. a) As-cast and b) Melt spun ribbon.

# END

# 5-81

# DTIC